

The Limits of Faint-Object Polarimetry

R. FOSBURY¹ (ST-ECF), A. CIMATTI (ESO/Florence, Italy)

S. DI SEREGO ALIGHIERI (Arcetri, Italy)

Introduction

A common problem in observational astrophysics is the investigation of complex geometrical structures which are below the resolution capabilities of telescopes. In some cases, small-scale structures can be inferred from the global morphology, e.g., the beautiful “ionization cones” seen in some of the nearby Seyfert galaxies (Figure 1), but a geometry-sensitive tool is needed in order to make real progress with the inference of the fundamental physical processes.

The study of rapid time variability has been valuable for the determination of physical scale sizes and, in some cases, the discovery of bulk relativistic effects as an explanation of apparent superluminal motion. It is polarimetry, however, which is capable of giving us the most detailed information about “directionality”. This is, of course, a well-established technique in astronomy with many applications in many wavebands. Polarimetric studies cover a wide range of astrophysical subjects. In particular, it is important for solar system objects, in many fields of stellar astrophysics (star-forming regions, young stars, binary systems, variable stars, pulsars, etc.) and in all extragalactic sources, from normal galaxies (magnetic fields, ISM) to active galaxies and QSOs (synchrotron emission, ISM, scattering, geometry). It is not our intention to review here either the applications or the physical processes and observing techniques. Rather it is to concentrate on a particular aspect of the subject which has yielded a rich harvest of new results on faint sources with the current generation of 4-m-class telescopes and promises even more from the yet-larger photon collectors which are just starting to become available. This is the study of the surroundings of active galactic nuclei (AGN) which show many indications of a predominantly axial symmetry determined by the properties of the fundamental source of luminosity.

Following the discovery of the “alignment effect” in high-redshift radio galaxies (HzRG) by McCarthy et al. (1987) and

by Chambers, Miley & van Breugel (1987), there has been considerable interest in trying to disentangle those components in the galaxies which can tell the story of their stellar evolutionary history from those which are the result of the presence of a powerful AGN. These objects show a roundish, red component and an irregular blue structure which is aligned – but not necessarily coincident – with the extended double radio source (Rigler et al. 1992, Dunlop & Peacock 1993). Attempts to explain the elongated blue component have centred on two mechanisms. One proposes that the particle jets which drive the extended radio source somehow trigger the formation of stars as they traverse the galaxy ISM (Rees 1989, De Young 1989). This young stellar population shines brightly in the UV and, rather like the track of a particle in a bubble-chamber, traces the radio axis before dynamical effects in the galaxy smear the structure. The second derives from the hypothesis that powerful radio galaxies and radio quasars are one and the same type of object and differ in appearance only by the inclination of the radio axis with respect to our line-of-sight. This unification scheme clearly implies the presence of a quasar nucleus in the HzRG which, as proposed by Tadhunter et al. (1988), will have profound effects on the ISM and will be impossible to hide – especially in the ultraviolet where the galaxy host may be relatively faint.

Optical observations of the HzRG with $z \geq 1$ sample the rest-frame UV and so it is not surprising that they show significant morphological differences from their (extremely rare) low redshift counterparts which are observed in the optical. One important question we have to answer, whatever the correct explanation of the alignment phenomenon, is whether these differences are *entirely* due to the different wavebands of the observations or whether we see evolutionary effects *in addition*. Our polarization observations have been directed towards testing the hypothesis that the blue, aligned structures result from the scattering of the nuclear quasar combined with locally generated line fluorescence excited by the EUV con-

tinuum. Clearly, the scattering will produce a linear polarization signature with a precisely defined geometry having the electric vector perpendicular to the direction of the illuminating source in the nucleus. This is a strong hypothesis since, with the appropriate observations, it is readily refutable.

Techniques

The determination of polarization demands the measurement of intensity ratios. For faint extragalactic sources, the fluxes from which the ratios are formed are measured in the presence of a strong, and generally polarized, sky background. Even small variations in this background would make sequential measurements of different polarization directions prone to severe systematic errors. The techniques in common use, therefore, make flux measurements in orthogonal polarization directions *simultaneously*. The method that we use with EFOSC1 (see *The Messenger*, September 1989, No. 57) for both imaging and spectro-polarimetry employs a Wollaston prism in the parallel beam and an aperture mask in the focal plane of the telescope. The mask ensures that the sky from one polarization is not superimposed on the object in the other (Figure 2).

We have used this method to measure polarizations in radio galaxies with redshifts as high as 2.63 and fainter than an R magnitude of 22. Our experience has been that, for these faint objects, the accuracy of the measurement is relatively free from systematic effects while the precision is entirely limited by counting statistics with CCD detectors. Instrumental polarization – which is <1% for imaging and <5% for spectropolarimetry – is straightforward to measure and correct for by looking at field stars and polarimetric standards. The critical part of the analysis is, fairly obviously, the extraction of the object flux – including faint extensions – from the background. Optimum methods for doing this, using high s/n sums of all the individual observations to define a weighting scheme, are being developed.

¹ Affiliated to the Astrophysics Division, Space Science Department, European Space Agency.

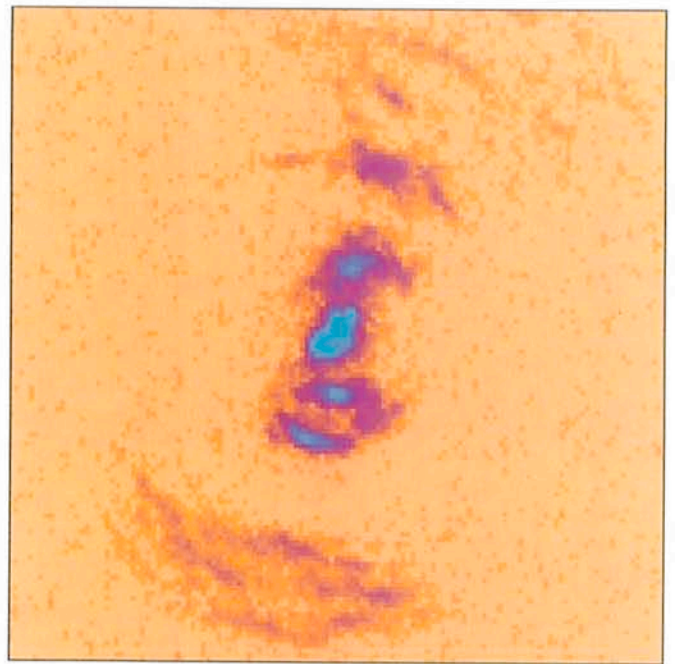
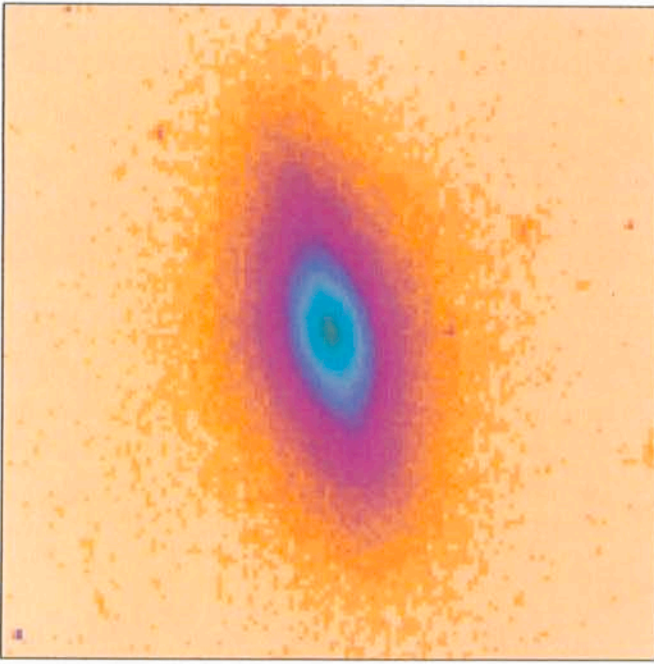


Figure 1 a: An example of ionization cones in the nearby Seyfert galaxy NGC5252 (Courtesy of Z. Tsvetanov & C. Tadhunter). The two images – with the same scale and orientation – show at the left line-free continuum (starlight) and at the right [OIII]5007 line emission (excited by the AGN).

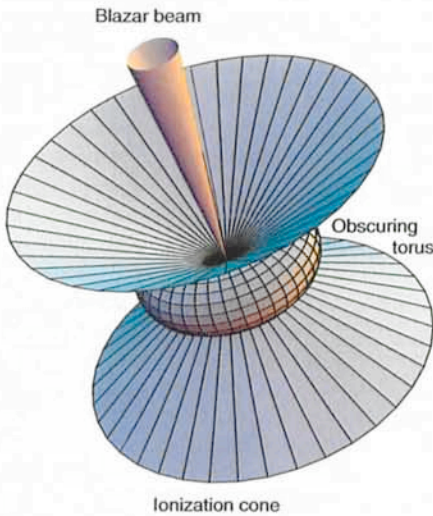


Figure 1 b: A cartoon of the origin of the ionization cone phenomenon by shadowing close to the AGN. In addition is shown the blazar beam which is thought to be produced by Doppler boosting in regions associated with the formation of the radio jet in radio galaxies. The radio-quiet Seyferts show no evidence of a blazar component.

Given our experience with the 3.6-m telescope, it is straightforward to extrapolate to the capability of an 8-m VLT element. The new, large telescopes are going to give enormous gains in this type of measurement and will allow detailed polarization mapping and high-resolution spectropolarimetry where now we struggle to do broad-band “aperture” polarimetry and coarse-resolution spectral measurements. The ability to reach galaxies at redshifts greater than one and to separate stellar and nuclear components will have profound

implications for our understanding of massive galaxy formation.

In recognition of the fact that the VLT will give very important gains for polarization measurements, most of the

planned instruments will have polarimetric capabilities which are briefly reviewed here.

FORS, an imager/spectrograph designed to work at the Cassegrain focus

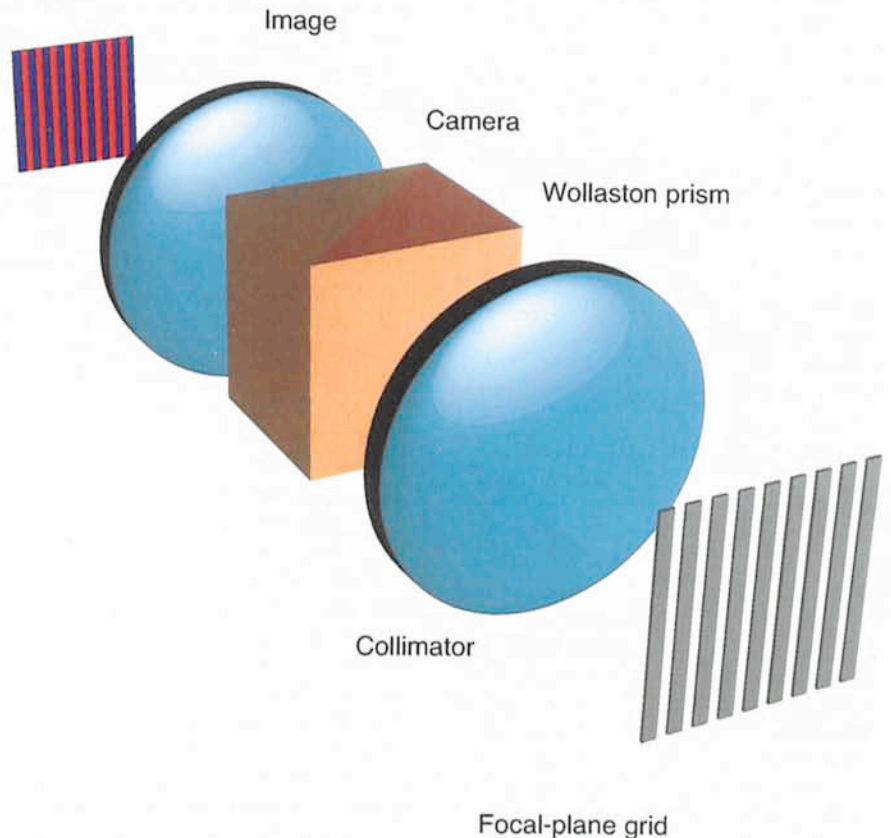


Figure 2: A schematic view of an imaging polarimeter using a Wollaston prism to split the polarized beams and a focal-plane mask to avoid overlapping images at the detector. At ESO, this facility is available with EFOSC and can be converted for spectropolarimetry by adding a grism in the parallel beam. An achromatic half-wave plate has been obtained and will shortly be added to the instrument so that the plane of polarization can be rotated with respect to the mask. This is especially important for spectropolarimetry.

between 330 and 1,100 nm with spectroscopic resolution up to 2000, will have both imaging- and spectropolarimetry modes. These are provided by rotatable retarders and a Wollaston prism to be used in combination with filters or grisms and focal plane masks or slitlets. It is anticipated that the degree of linear polarization will be measured with an accuracy of 1% in one hour down to U, B, V and R magnitudes of 22–23 in imaging and down to $V=17.3$ in spectroscopy with 2.5\AA resolution.

ISAAC, the IR imager/spectrograph for the Nasmyth focus will work between 1 and $5\mu\text{m}$ with spectroscopic resolutions in the range 300–10,000. It will do imaging polarimetry using a fixed analyser in one of the filter wheels, to be used in combination with filters and with rotation of the whole instrument.

Similarly, imaging polarimetry will be possible with CONICA, the high spatial resolution, near-IR ($1\text{--}5\mu\text{m}$) camera. This is designed to work at the coudé focus in combination with adaptive optics but the effects of the coudé optical train on polarization measurements have yet to be carefully assessed.

UVES is an echelle spectrograph for the Nasmyth with a spectroscopic resolution of 40,000. The possibility of doing spectropolarimetry with a polarization analyser in the pre-slit optical train has been investigated, but is not in the present plan because of possible difficulties with the polarization induced by M3, the image slicer, the image derotator and the spectrograph. Nevertheless these problems are not insoluble and polarimetry with UVES would be useful, e.g., to study the line polarization structure in AGN.

The present design of the $10\text{--}20\mu\text{m}$ Cassegrain imager/spectrograph anticipates that both imaging- and spectropolarimetry will be possible with a rotatable retarder and fixed analyser.

Simulation and Error Estimates

The state of polarized light is described by the four Stokes parameters, I , Q , U and V . These can be normalized to unit intensity for the light source and it is then the second two components of the vector, q and u from which the state of linear polarization is derived. In a practical polarimeter, q and u are represented by appropriate intensity ratios in orthogonal polarizations. When poisson noise from the object and the sky is the only source of error, the distribution functions of q and u are straightforward to calculate and only become non-normal at very low signal/noise ratios (Clarke et al. 1983). The quantities of direct astrophysical interest, the degree of polarization p and

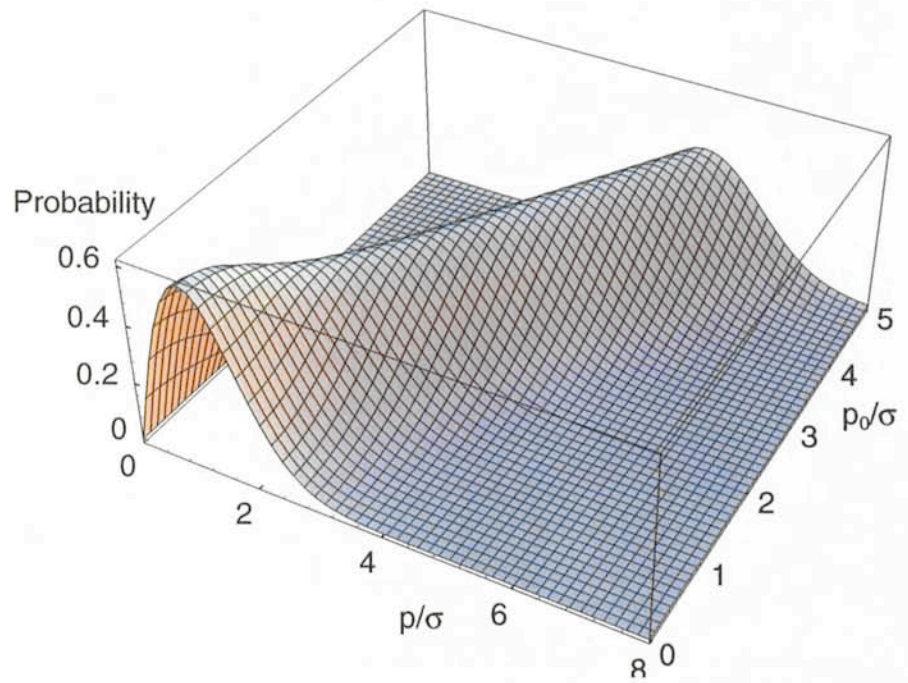


Figure 3: A three-dimensional plot of the analytic distribution function (a Rice distribution) for the linear polarization measured in the presence of poisson noise. The x-axis shows the measured polarization (normalized to the observational σ), while the y (depth)-axis shows the similarly normalized true (input) polarization. The distribution becomes highly skewed as $p/\sigma \rightarrow 0$ and so the resulting measurement bias must be removed.

the orientation of the electric vector ϑ , are derived from q and u as their quadratic sum and the arctangent of their ratio respectively. The distribution functions of p and ϑ are no longer normal and that of p becomes skewed as $p \rightarrow 0$ (Figure 3). These distribution functions have to be calculated, either analytically or by Monte-Carlo simulation, before proper confidence limits can be attached to measurements (Simmons & Stewart 1985, Clarke & Stewart 1986). Because of its skewed distribution, measurements of p close to zero are biased and this has to be removed using the calculated distribution function (Wardle & Kronberg 1974).

While the analytic functions can be used to reduce observations, we have found it convenient to build a stochastic model of the polarimeter which can be readily adjusted to match a particular observational setup and set of measurement angles. In addition to calculating the distribution functions for the quantities of interest, the simulation can be used to optimize the use of a given amount of observing time amongst a sequence of exposures at different orientations of the polarizing prism. Our version is implemented in the Interactive Data Language (IDL) and runs on a Sun workstation. A typical run of 30,000 trials for a set of four angles takes just a few minutes on a Sparc 10. The sample output shown in Figure 4 represents a set of imaging observations of the $z=2.63$ galaxy MRC2025-218 (Cimatti

et al. 1993b). In this case, q and u are the amplitudes of the sine and cosine terms in a sinusoidal fit to a set of intensity ratios at different orientation angles of the instrument. The bias in the measurement of p is obtained by comparing the value input to the simulation with that derived from fitting the peak of the p -distribution. These observations used a total observing time of 270 min on the 2.2-m and 3.6-m telescopes and are close to the limit of what can be achieved with these instruments. The same precision could be reached in less than an hour with the same type of instrumentation on an 8-m telescope.

Scientific Highlights

The first detection of polarization in HzRG with $z > 1$ was in 3C386 and 3C277.2 (di Serego Alighieri et al. 1989) and this was followed by a polarization map of 3C368 made by the Durham group (Scarrott, Rolph & Tadhunter 1990). There are now measurements of some forty objects with $z > 0.1$ (Cimatti et al. 1993a) and a remarkably well-defined trend is emerging. The degree of linear polarization is strongly correlated with the rest wavelength of the observed radiation (Figure 5). For a given filter, this manifests itself as a correlation with redshift but it appears that the wavelength dominates any evolutionary effects (Cimatti et al. 1993a). For those objects observed at a rest wavelength below 4000\AA , the polariza-

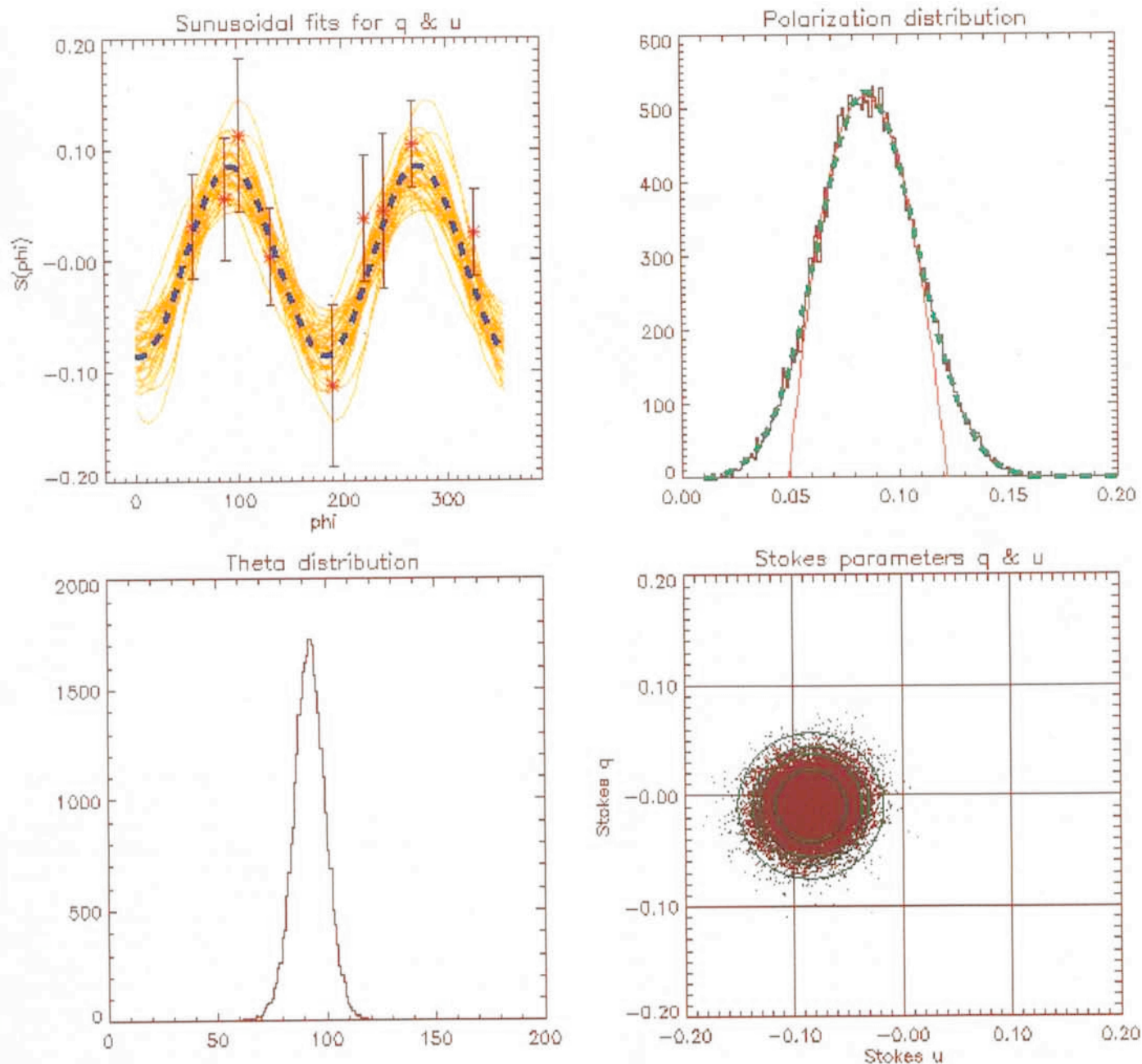


Figure 4: A representation of our stochastic model of imaging polarimetry. This shows the measured data for the high redshift radio galaxy MRC2025-218 ($z=2.63$) from the ESO 2.2 and 3.6-m telescopes. In clockwise order, the four frames show: (1) The measured data points with their 1 s error bars (red stars) and the fitted sinusoid (blue dashes). The yellow curves represent every thousandth fit to 30,000 simulated data sets with poisson noise added to sky and object counts. (2) The polarization distribution resulting from the simulations. The gaussian (green) and paraboloidal (red – fitted to the peak only) fits are used for finding the most probable polarization. This measurement corresponds to a p/s of 3.8 and so the distribution function differs only slightly from a normal curve. (3) The distribution function for the position angle of the E-vector. (4) The distribution of simulated points in the q, u-plane. The circles represent 67 %, 90 % and 95 % confidence limits.

tion is generally higher – ranging up to 20% – than the objects observed at longer wavelengths and has an E-vector which is, in all measured cases, perpendicular to the radio axis within the measurement error.

Spectropolarimetry (di Serego Alighieri, Cimatti & Fosbury 1993 and in preparation) shows this polarization drop longward of 4000\AA very clearly in two individual objects. This is interpreted as the increasing dominance of unpolarized starlight above the H&K-break from an old stellar population (Figure 6).

Attempts to model the spectral energy distributions and polarizations of these HzRG using a combination of starlight and scattered quasar light are hampered by the paucity of spectropolarimetric – or line-free imaging polarimetric – data. They do, however, indicate that it is possible to reproduce these two types of measurement simultaneously using an old stellar population and scattering by dust. Electron scattering cannot, however, be ruled out and remains a possibility especially close to the nucleus and, possibly, for sources in rich clusters.

Taken with other tests of the radio-loud unification scheme, the polarimetry provides very strong evidence that the HzRG indeed harbour obscured quasar nuclei. Many details, however, remain to be investigated. For example, it is not known how much the blazar beam – thought to be present in all radio-loud quasars – contributes to the scattered radiation. This will have a bearing on the relative strength of any scattered broad-line radiation. There is also evidence that the non-stellar continuum radiation from AGN may be as extended or even more extended than the BLR (Binette,

Fosbury & Parker 1993, Antonucci 1993) which will also have an effect on the ratio of line to continuum radiation in polarized light.

Conclusions

Both imaging and spectropolarimetry are now playing an important role in the understanding of the AGN phenomenon. We have discussed here only the polarization produced by scattering. Intrinsically polarized emission mechanisms like synchrotron radiation are also, of course, the subject of intensive study in these objects. The nearby Seyfert galaxies can now be studied in great detail using polarimetric techniques, and we fully expect to be able to emulate such investigations at cosmologically interesting distances when we have access to the bigger telescopes. The extension of the measurements into the infrared will also be interesting, especially for resolving the electron vs. dust scattering question.

Finally, we stress that the use of spectropolarimetry to identify and remove the AGN contribution to the luminosity of very distant radio galaxies can allow deductions to be made about their stellar evolutionary histories with much greater confidence than pure spectroscopy. The epoch of galaxy formation is one of the outstanding questions in cosmology today.

References

Antonucci, R., 1993. In: IAU Symposium #159. "Active galactic nuclei across the electromagnetic spectrum", Geneva, 1993.
 Binette, L., Fosbury, R.A.E. & Parker, D., 1993. *PASP*, **105**, 1150.
 Chambers, K.C., Miley, G.K., & van Breugel, W. 1987, *Nature*, **329**, 604.

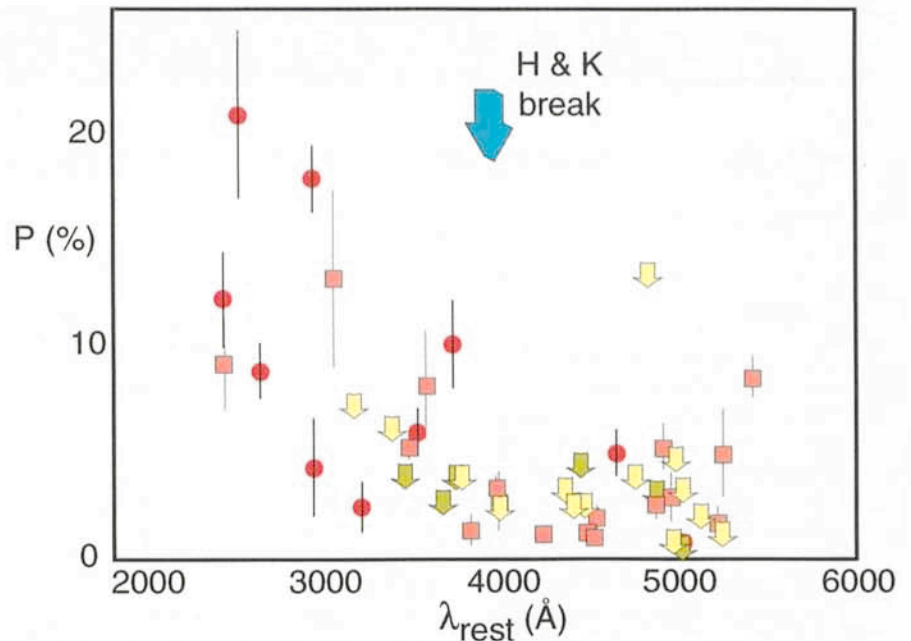


Figure 5: Linear polarization measurements for radio galaxies with $z > 0.1$ collected by Cimatti et al. (1993a). The arrows represent upper limits and the different symbols are from different observers. The fractional polarization is plotted against the wavelength of the filter passband in the rest-frame of the galaxy. All the detected polarizations to the left of the H&K break have E-vectors perpendicular to the radio axis.

Cimatti, A., di Serego Alighieri, S., Field, G.M., G.M. & Fosbury, R.A.E., 1993b, *ApJ*, in press.
 Cimatti, A., di Serego Alighieri, S., Fosbury, R.A.E., Salvati, M., & Taylor, D. 1993a, *MNRAS*, **264**, 421.
 Clarke, D. & Stewart, B.G., 1986. *Vistas in Astron.* **29**, 27.
 Clarke, D., Stewart, B.G., Schwarz, H. E. & Brooks, A., 1983. *A&A*, **126**, 260.
 De Young, D.S. 1989. *ApJ*, **342**, L59.
 di Serego Alighieri, S., Fosbury, R.A.E., Quinn, P.J. & Tadhunter C.N., 1989. *Nature*, **341**, 307.
 di Serego Alighieri, S., Cimatti, A., Fosbury, R.A.E., 1993, in *Active Galactic Nuclei across the Electromagnetic Spectrum*, Courvoisier et al. eds., in press.

Dunlop J.S., Peacock J.A., 1993, *MNRAS*, in press.
 McCarthy P.J., van Breugel W., Spinrad H. & Djorgowski S., 1987. *Ap J*, **321**, L29.
 Rees, M., 1989. *MNRAS*, **239**, 1p.
 Rigler, M.A., Lilly, S.J., Stockton, A., Hammer, F. & Le Fèvre, O., 1992, *Ap J*, **385**, 61.
 Scarrott, S.M., Rolph, C.D. & Tadhunter, C.N., 1990. *MNRAS*, **24**, 5p.
 Simmons, J.F.L. & Stewart, B.G., 1985, *A&A*, **142**, 100.
 Tadhunter, C.N., Fosbury, R.A.E., di Serego Alighieri, S., 1988. In: "BL Lac Objects", Maraschi, L., Maccacaro, T. & Ulrich, M-H., eds. Springer-Verlag, Berlin, p. 79.
 Wardle, J.F.C. & Kronberg, P.P., 1974. *Ap J*, **194**, 249.

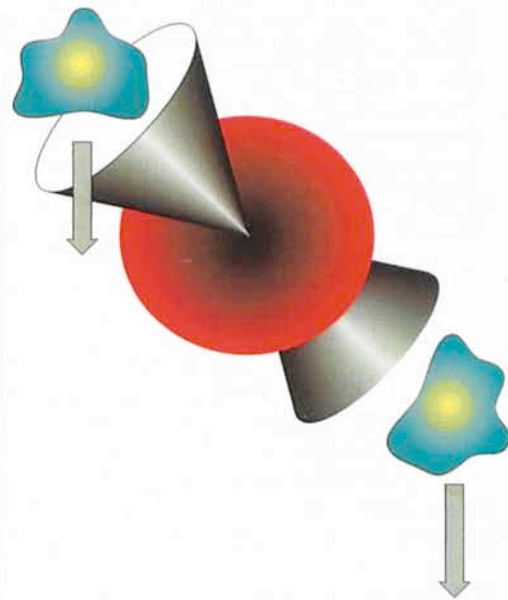
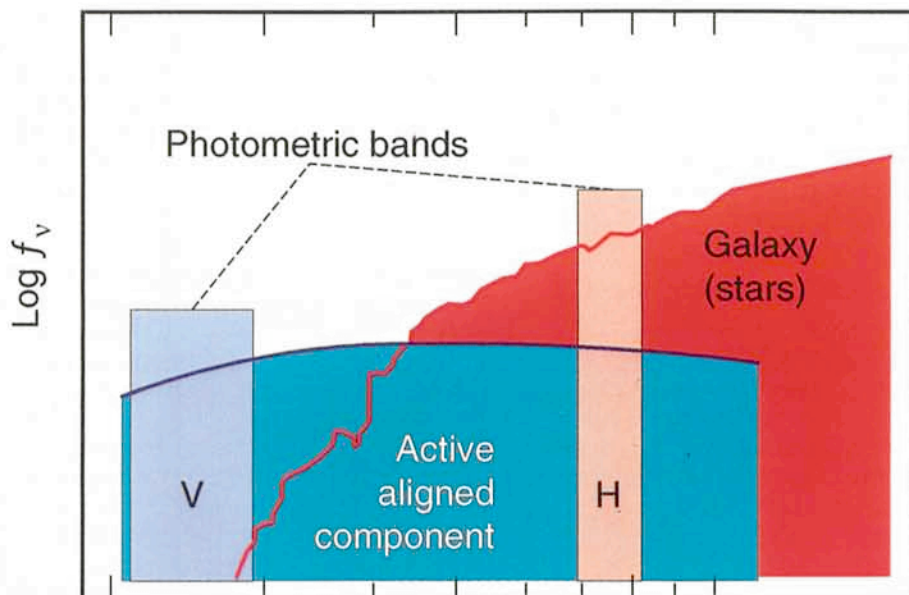


Figure 6: A cartoon of the spectral energy distribution of a HzRG adapted from Rigler et al. (1992). This shows the two spectral components which will alternatively dominate the measured flux above and below the H&K break in the restframe of the galaxy. We identify the blue component with the alignment effect which results from fluorescence and scattering processes powered by the AGN.